minerals

MDPI

Article

Ammonium-Bearing Fluorapophyllite-(K) in the Magnesian Skarns from Aleului Valley, Pietroasa, Romania

Ştefan Marincea [1,*], Delia-Georgeta Dumitraş [1], Cristina Sava Ghineţ [1], Andra Elena Filiuţă [1], Fabrice Dal Bo [2], Frédéric Hatert [2] and Gelu Costin [3]

[1] Department INI, Geological Institute of Romania, 1 Caransebeş Str., 012271 Bucharest, Romania; d_deliaro@yahoo.com (D.-G.D.); ghinet.cristina@yahoo.com (C.S.G.); f.e_andra@yahoo.com (A.E.F.)
[2] Laboratoire de Minéralogie, Université de Liège, Sart-Tilman, Bâtiment B 18, B-4000 Liège, Belgium; fabrice.dalbo@gmail.com (F.D.B.); fhatert@ulg.ac.be (F.H.)
[3] Department of Earth, Environmental and Planetary Sciences, Rice University, Houston, TX 77005, USA; g.costin@rice.edu
* Correspondence: smarincea@yahoo.com or marincea@igr.ro

Abstract: An ammonium-bearing fluorapophyllite-(K) occurs as a late hydrothermal product in the outer endoskarn zone from Aleului Valley (N 46°37′04″, E 22°35′22″), located at the contact of the granodiorite laccolith from Pietroasa, of Upper Cretaceous age, with Anisian dolostones. Associated minerals are wollastonite, K feldspar, diopside, fluorapatite, talc, and pectolite. The chemical structural formula is $[K_{0.985}Na_{0.012}(NH_4)_{0.076}]_{\Sigma=1.073}(Ca_{4.009}Mn_{0.001}Fe^{2+}{}_{0.003}Mg_{0.002}Ba_{0.001})_{\Sigma=4.016}(Si_{7.953}Al_{0.047})O_{20.029}[F_{0.899}(OH)_{0.101}]\cdot 8.059H_2O$. The structure was successfully refined as tetragonal, space group $P4/mnc$, with cell parameters of a = 8.9685(1) Å and c = 15.7885(5) Å. The indices of refraction are ω = 1.534(1) and ε = 1.536(1). The calculated density is D_x = 2.381 g/cm^3, in good agreement with the measured density, D_m = 2.379(4) g/cm^3. The thermal analysis shows that the mineral completely dehydrates at up to 450 °C (endothermic effects at 330, 371, and 448 °C) and loses ammonium at 634 °C. In the infrared spectra, the multiplicity of the bands assumed to be silicate modes ($1\nu_1 + 3\nu_3 + 2\nu_2 + 3\nu_4$) agrees with the reduction in the symmetry of the $SiO_4{}^{4-}$ ion from T_d to C_δ. Fluorapophyllite-(K) from Aleului Valley is of late hydrothermal origin and crystallized from F-rich fluids originating from the granodiorite intrusion, which mobilized K, Ca, and Si from the pre-existing feldspar.

Keywords: fluorapophyllite-(K); physical properties; crystal chemistry; structure; Raman spectra; FTIR; thermal analysis; endoskarn; late hydrothermalism; Pietroasa laccolith (Romania)

Citation: Marincea, Ş.; Dumitraş, D.-G.; Sava Ghineţ, C.; Filiuţă, A.E.; Dal Bo, F.; Hatert, F.; Costin, G. Ammonium-Bearing Fluorapophyllite-(K) in the Magnesian Skarns from Aleului Valley, Pietroasa, Romania. *Minerals* **2023**, *13*, 1362. https://doi.org/10.3390/min13111362

Academic Editor: Jaroslav Pršek

Received: 19 September 2023
Revised: 17 October 2023
Accepted: 23 October 2023
Published: 25 October 2023

1. Introduction

Fluorapophyllite-(K) [1] represents the most common mineral of the apophyllite group. The mineral, ideally $KCa_4(Si_8O_{20})F\cdot 8H_2O$, is tetragonal, space group $P4/mnc$, and forms a continuous solid-solution series with hydroxyapophyllite-(K), ideally $KCa_4(Si_8O_{20})(OH)\cdot 8H_2O$, and apparently with two other minerals that crystallize in the same space group, fluorapophyllite-(Cs) [2] and fluorapophyllite-(NH_4) [3]. Hydroyapophyllite-(K) and, consequently, fluorapophyllite-(K) are also isostructural with hydroxymcglassonite-(K), where Sr substitutes for Ca [4]. The isomorphism toward the orthorhombic *Pnnm* members of the group, i.e., fluorapophyllite-(Na) and hydroxyapophyllite-(Na), is restricted by the differences in symmetry and seems to define a pseudo-solid solution series [5,6].

Fluorapophyllite-(K) is a low-temperature mineral that generally occurs as fillings of vugs and veins in calc alkaline basic rocks or other basic systems, where it associates mainly with zeolite-group minerals but also as a retrograde skarn mineral (e.g., [7–13]). In this second case, the mineral characteristically associates with primary skarn minerals (e.g., wollastonite, datolite, Ca-garnet) being the product of the retromorphic evolution ("dissolution–reprecipitation processes" according to [8]).

Fluorapophyllite-(K) in the skarn from Aleului Valley was first identified by [10] and misidentified as hydroxyapophyllite-(K) based on a bulk (wet chemical) analysis. The mineral occurs in a typical skarn association. The opportunity to re-analyze the mineral, as well as a supplement of the material available for new study, prompted re-investigation of the mineral, which resulted in this paper.

2. Geological Setting

As mentioned before, a mineral in the solid-solution series fluorapophyllite-(K)–hydroxyapophyllite-(K) was described in the magnesian skarn from Aleului Valley by [10], who also offered a description of this proximal skarn. The mineral occurs on vugs and fractures that affect the skarn mass. The host skarn occurs in the close vicinity of the western contact of the Pietroasa intrusive body with Anisian dolostones pertaining to the Ferice Unit, at approximately 500 upstream from the confluence of Sebişel with Aleului Valleys, on the right slope of Aleului (Figure 1).

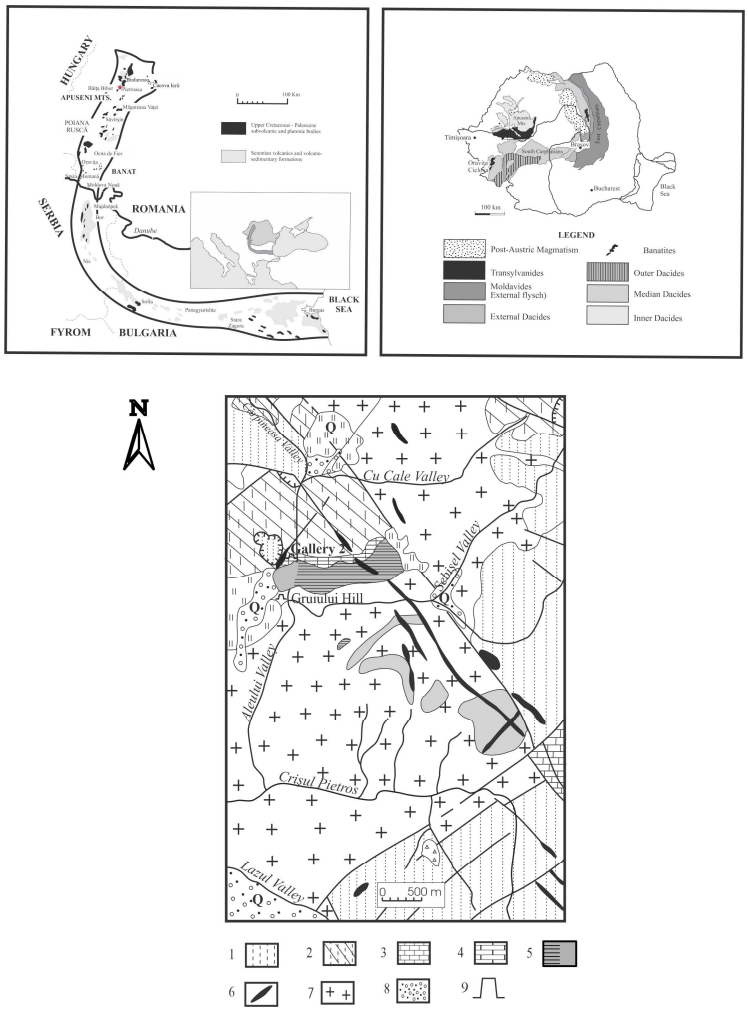

Figure 1. Geological sketch of Pietroasa area in regional context: The Banatitic Magmatic and Metallogenetic Belt (top, left: redrawn from [14]) and the structural context of Romania (top, right: from [15], simplified). Redrawn and modified from [16]. Symbols in the legend represent Ferice Unit 1—Werfenian (siliciclastic rocks); 2—Anisian (dolostones and dolomitic limestones); Bătrânescu Unit: 3—Ladinian (limestones); Bihor Unit: 4—Lower and Middle Jurassic (schistose clays, sandstones, and black limestones); 5—Dolomitic marbles, magnesian skarns, and hornfelses; 6–7—Upper Cretaceous magmatites ("banatites"); 6—vein rocks of rhyolitic, andesitic, or basaltic composition; 7—granodiorites, granites; 8—Quaternary alluvial and delluvial deposits (muds, gravels, sands); 9—gallery. The star marks the location of Aleului 2 Gallery.

The skarn, investigated with an exploration mine shaft, mainly consists of a mass of forsterite, minerals of the humite group (chondrodite, clinohumite), diopside, spinel, and phlogopite, in a matrix of serpentine (chondrodite, lizardite), chlorite, and carbonates (calcite, dolomite). The coordinates of the shaft entry, dug in the late 1980s and known as "Galeria 2 (Gallery 2 or Adit 2) Aleului", are N 46°37′04″, E 22°35′22″. A body of distal, boron-bearing magnesian skarn containing suanite, kotoite, ludwigite, and szaibelyite was described in the closest vicinity, at approximately 500 m downstream, at the point called "Gruiului Hilll": [10,17–19].

The intrusive body from Pietroasa, responsible for the thermal metamorphism and skarn formation, is a laccolith that represents the eastern occurrence of the Bihor Batholith, likely the most important from a metallogenetic point of view in the Banatitic Magmatic and Metallogenetic Belt [20]. This Belt consists of a series of discontinuous magmatic and metallogenetic districts that are discordant over a Middle Cretaceous-aged nappe structure ([14,21,22] and references therein), as shown in Figure 1. The laccolith from Pietroasa consists mainly of granodiorite and granite porphyry with subordinate quartz monzodiorite and microdiorite [23,24]. The K-Ar age on the mafic fraction reported by [16] is 74(3) to 67(3) Ma, in fair agreement with the ages compiled by [21]: 73(3) to 70(3) Ma.

Fluorapophyllite-(K) occurs in vugs, but also as infilling of fractures that cross-cut the magnesian skarns in both the exoskarn and endoskarn zones. The crystals of fluorapophyllite-(K) contain small inclusions of wollastonite, pectolite, fluorapatite, and K feldspar, and are sometimes crosscut by small veins of diopside with talc overcoats (Figures 2 and 3).

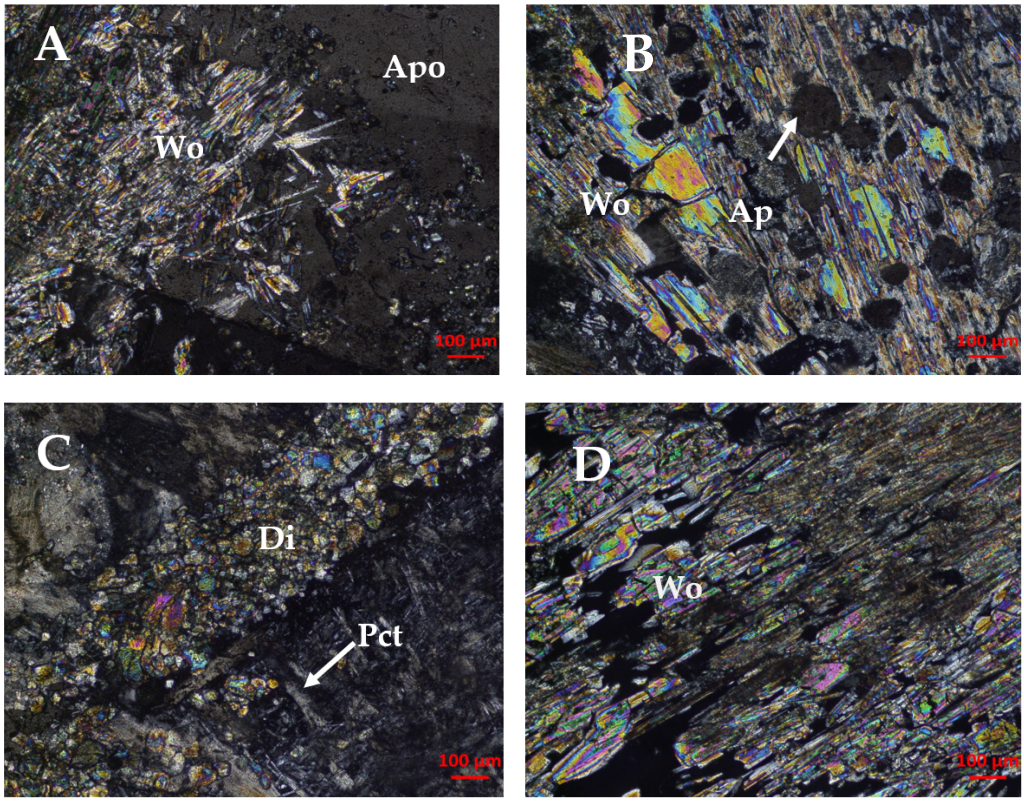

Figure 2. Photomicrographs showing characteristic relationships between fluorapophyllite-(K) and associated minerals in the Aleului Valley skarn. Crossed polars. The scale bar on each photograph represents 0.1 mm. (**A**) Aggregate of wollastonite (Wo) crystals engulfed by fluorapophyllite-(K) (Apo). (**B**) Wollastonite (Wo) and fluorapatite (Ap) in the fluorapophyllite-(K) mass. (**C**) Vein of diopside (Di) cutting an aggregate of fluorapophyllite-(K) and pectolite (Pct). (**D**) Detail of an aggregate of wollastonite (Wo). Symbols for the rock-forming minerals follow the recommendations of [25].

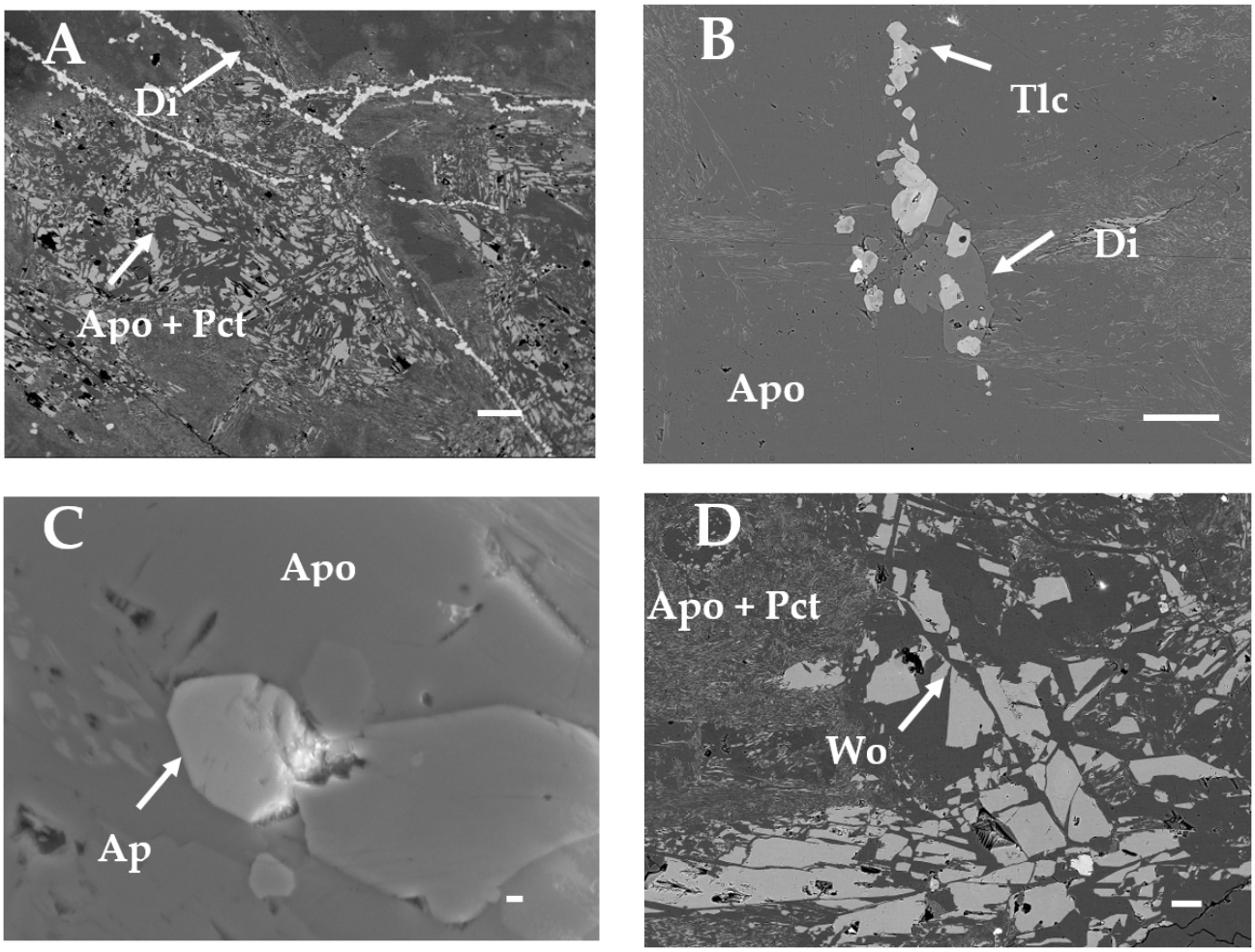

Figure 3. SEM-BSE microphotographs of typical associations of fluorapophyllite-(K) from Aleului Valley. The scale bar on the photographs represents 100 μm (**A**,**B**,**D**) and 10 μm, respectively (**C**). The symbols are the same as in Figure 2, except for Tlc = talc.

3. Materials and Methods

Electron-microprobe analyses (EMPA) were performed using a Jeol JXA 8530F Hyperprobe (JEOL Ltd., Tokyo, Japan), equipped with a field emission-assisted thermo-ionic (Schottky) emitter, five wavelength-dispersive spectrometers (WDS), and one SD EDS detector. The apparatus is hosted by Rice University, Department of Earth, Environment, and Planetary Science (Houston, TX, USA). The apparatus was set at an accelerating voltage of 15 kV and a beam current of 20 nA (measured at the Faraday cup), for beam diameters of 5–20 μm (smaller for fluorapatite and talc because of the small size of crystals). A defocused beam (20 μm) was used for the analysis of Na and K to avoid their loss. Natural plagioclase—An 67 (Si and Ca Kα), natural olivine—Fo 93 (Mg and Fe Kα), natural orthoclase (K and Al Kα), natural jadeite (Na Kα), natural celestite (Sr Kα), natural Ce-monazite (La, Nd and Ce Kα), natural baryte (Ba Kα), natural topaz (F Kα), and natural tugtupite (Cl Kα) served as standards. Counting time was 20 s per element. Data were reduced using the Phi-Rho-Z matrix correction [26]. Ammonium was determined by colorimetry from a separate aliquot dissolved in 1 M HCl, using the Nessler reagent [27].

The fast identification of mineral phases in all samples was performed by Energy-Dispersive Spectrometry (EDS) analysis, using a JEOL Silicon Drift (SD) X-ray Detector with 10 mm^2 active area and 133 eV resolution. The detector is attached and integrated into a JEOL JXA 8530F Hyperprobe. The analytical conditions used for EDS analysis were as follows: 15 kV accelerating voltage, 20 nA beam current, live time 20 s. Dead Time (DT)

during the analysis was 35%–40% with count rates ranging from ~45,000 to ~100,000. The beam size used was "spot" size (~300 nm).

Supplementary high-resolution SEM images were obtained at the Geological Institute of Romania, using a Hitachi TM3030 tabletop scanning electron microscope (Chiyoda, Tokyo, Japan), with an improved electron optical system, operated at 5 kV acceleration voltage.

The XRD patterns of two representative samples (212 and 213, respectively) were recorded using two different Brucker (AXS) D8 Advance diffractometers (Karlsruhe, Germany) hosted by the Laboratory of Mineralogy, University of Liège (Belgium) and Geological Institute of Romania (Bucharest), respectively. Both diffractometers used Ni-filtered Cu$K\alpha$ radiation, a step size of 0.02° 2θ, and a counting time of 6 s per step. An operating voltage of 40 kV for a current of 30 mA, a slit system of 1/0.1/1 with a receiving slit of 0.6 mm, and a scanning range of 4 to 100° 2θ were used for measurements. For both samples, the unit-cell parameters were calculated by least-squares refinement of the XRD data, using the computer program of [28] modified by [29]. Synthetic silicon (NBS 640b) was used as an external standard in order to verify the accuracy of measurements.

The structure refinement was performed by single-crystal X-ray diffraction. Data were collected at room temperature with monochromatized Mo$K\alpha$ radiation (λ = 0.71703 Å—50 kV and 1 mA) on a Rigaku Agilent Xcalibur EOS diffractometer equipped with a CCD Detector (both manufactured in Osaka, Japan), housed at the Laboratory of Mineralogy, University of Liège. The instrument has Kappa geometry. Data collection, subsequent data reduction, and face-based absorption corrections were carried out using CrysAlis Pro 41.123a software [30]. The initial structure solution in space group $P4/mnc$ was determined by the charge flipping method using the Superflip algorithm [31], and the structural model was subsequently refined on the basis of F^2 with Jana2006 software [32].

DTA and TG simultaneous records were made using a NETZSCH STA thermobalance (Netzsch-Gerätebau GmbH, Selb, Germany), hosted by the Geological Institute of Romania. The apparatus was operated in the temperature range of 25–1100 °C, in air flow, at a heating rate of 5 °C/min. An Al_2O_3 crucible was used for the analysis. Furthermore, 333 mg of carefully handpicked fluorapophyllite-(K) crystals were crushed and used as the starting material.

The infrared absorption spectra were obtained using both a Fourier-transform THERMO Nicolet Nexus spectrometer (ThermoFisher Scientific, Madison, WI, USA), hosted by the University of Liège (for Sample 212), and a BRUKER FTIR S 12 spectrometer (Ettlingen, Germany) hosted by the Geological Institute of Romania (for Sample 213). Both records were made in the frequency range between 400 and 4000 cm^{-1}, using a standard pressed-disk technique, after embedding 2 mg of mechanically ground mineral powder in 148 mg of dry KBr and compacting under 2500 N/cm^2 pressure. The spectral resolution was, in both cases, 0.1 cm^{-1}. The spectra were recorded at 25 °C.

Raman spectra were recorded using a Renishaw SEM-Raman system (Artisan Scientific, Champaign, IL, USA) hosted by the Geological Institute of Romania, at 25 °C, using both structural and chemical analyses (SCA) and inVia interfaces. The spectrometer was equipped with a 10 mW, 532 nm diode-pumped solid-state laser as an excitation source. The spectral resolution was 1cm^{-1} for a 1 μm spatial resolution. Analyses were performed using a 50× objective, a confocal aperture of 400 μm, a 150 μm slit width, and 1800 lines·mm^{-1} grating. Repeated acquisitions on the crystals were accumulated to improve the signal-to-noise ratio of the spectra, which were collected in the range of 100–4000 cm^{-1} (10-s accumulation time, 3 scans). The instrument was calibrated with synthetic silicon and fluorapatite.

The mean density of various crystals of fluorapophyllite-(K) was measured using a pycnometer (Rainhard Co., Austin, TX, USA), at 25 °C, using a mixture of methylene iodide and toluene as the immersion liquid.

Indices of refraction were measured at room temperature (25 °C), using the Becke-line method and monochromatic (Na) light (λ = 589 nm), by immersion in Cargille oils, using a spindle stage and a JENAPOL-U microscope (Carl Zeiss, Jena, Germany).

UV-luminescence tests were performed using a portable Vetter ultraviolet lamp (Vetter, Lottstetten, Germany) with 254 and 366 nm filters.

4. Associated Minerals

As mentioned by [10], wollastonite occurs as aggregates of needle-like crystals grouped in sheaves or bands inside the fluorapophyllite-(K) crystals, which maintain their optical continuity (Figure 2A,B,D). The individual crystals are up to 0.25 mm in length. The chemical composition of wollastonite, taken as an average of 14 different electron microprobe point analyses, is (in wt.% oxides) SiO_2 = 51.98, Al_2O_3 = 0.01, MgO = 0.02, CaO = 48.51, FeO = 0.02, Total = 100.54. The corresponding chemical-structural formula, calculated on the basis of 18(O) anions, is $(Ca_{5.997}Mg_{0.003}Fe^{2+}{}_{0.002})(Si_{5.998}Al_{0.001})O_{18}$. As expected, the composition conforms closely to stoichiometry. No significant compositional variation is observed either within individual crystals or inside the crystals.

Pectolite occurs as small fringes randomly distributed inside the fluorapophyllite-(K) crystals and has the tendency to form bands or sectors with apparent optical continuity (Figure 2C). The individual crystals, up to 20 μm in length, have silk-like development and low birefringence, but are easy to distinguish from fluorapophyllite-(K) due to their higher indices of refraction (positive relief). The association between pectolite and fluorapophyllite-(K) fully occupies sectors of fluorapophyllite-(K) crystals (Figure 3A,B,D).

The average chemical analysis obtained as a result of 45 point analyses performed by EMPA on three different crystals of pectolite included by the fluorapophyllite-(K) mass is (in wt.% oxides) SiO_2 = 54.29, CaO = 33.89, MgO = 0.01, MnO = 0.11, FeO = 0.04, BaO = 0.02, Na_2O = 8.95, K_2O = 0.05, F = 0.07, Cl = 0.01, H_2O (calculated) = 2.65, (F, Cl) = O = −0.01, Total = 100.08. Normalized to 8 (O) and 1 (OH, F, Cl) anions, this yields to the formula $(Na_{0.958}K_{0.004}Ca_{0.037})(Ca_{1.970}Mg_{0.001}Mn_{0.005}Fe_{0.002})Si_{3.002}O_8(OH_{0.980}F_{0.003}Cl_{0.017})$.

As pectolite was not described in skarns from Romania, apart from the syenite-like endoskarn from Măgureaua Vaţei [33], a detailed look at the chemistry is given as supplementary material (Table S1).

Diopside occurs as a relic mineral on veins that cut the fluorapophyllite-(K) mass (Figures 2 and 3). The individual crystals, up to 0.1 mm in length, are subhedral and sometimes lined by talc. The average composition, taken as the mean of 33 EMP analyses performed on 12 different crystals, is (in wt.% oxides) SiO_2 = 52.77, Al_2O_3 = 0.06, CaO = 23.29, MgO = 12.26, MnO = 0.17, FeO = 9.25, Na_2O = 1.54, K_2O = 0.04, Total = 99.38, yielding, by normalization to 6 (O) anions, the formula $(Ca_{0.946}Mg_{0.693}Fe^{2+}{}_{0.293}Mn_{0.005}Al_{0.060}Na_{0.113}K_{0.002})Si_{2.000}O_6$. Part of iron, considered to be in a divalent state of oxidation, must be, in reality, oxidized to Fe^{3+}. The composition below corresponds to a diopside (63.55 mol.%) with significant contents of hedenbergite (25.40 mol.%) and aegirine (10.55 mol.%) and minor johansennite (0.46 mol.%) and esseneite (0.05 mol.%).

K-feldspar (microcline) was found as small (up to 50 μm across), subhedral relics surrounded or engulfed by the fluorapophyllite-(K) mass. The average composition, taken as the mean of four point analyses performed on different crystals, is (in wt.% oxides) SiO_2 = 64.32, Al_2O_3 = 17.49, CaO = 0.07, MgO = 0.01, MnO = 0.01, FeO = 0.64, Na_2O = 0.42, K_2O = 16.05, Total = 99.01.

Normalized to 8 (O) anions, this composition results in the formula $(K_{0.959}Na_{0.038}Ca_{0.004}Fe^{2+}{}_{0.025}Mg_{0.001})(Al_{0.965}Si_{0.012})Si_3O_8$.

Talc occurs as a usual alteration product of diopside, generally as flakes lining diopside aggregates and crystals, inside or at the periphery of the diopside veins. Individual aggregates of talc were, however, identified (Figure 3B) and likely express the complete replacement of the pre-existing clinopyroxene. The mean chemical composition taken as the average of 27 EMP point analyses is (in wt.%) SiO_2 = 60.69, Al_2O_3 = 0.01, Cr_2O_3 = 0.01, MgO = 30.18, CaO = 0.92, MnO = 0.18, FeO = 0.07, Na_2O = 0.04, K_2O = 0.20, H_2O (calculated) = 4.81, Total = 97.11. The corresponding chemical-structural formula, calculated on the basis of 7 cations excluding H^+ and 12 (O,OH), is $(Mg_{2.397}Ca_{0.064}Mn_{0.010}Fe_{0.004}Na_{0.005}K_{0.017})(Si_{3.962}Al_{0.001}Cr_{0.001})O_{11.906}(OH)_{2.094}$.

Fluorapatite was identified as euhedral to subhedral crystals surrounded by fluorapophyllite-(K). Individual crystals are up to 100 μm in length, usually being much smaller. Representative images are given in Figures 2A and 3C. The chemical composition, taken as the average of 11 EMP point analyses on three different crystals, is (in wt.% oxides) P_2O_5 = 41.53, SO_3 = 0.45, La_2O_3 = 0.09, Ce_2O_3 = 0.11, Nd_2O_3 = 0.05, CaO = 55.05, Na_2O = 0.03, F = 3.16, Cl = 0.08, H_2O (calculated) = 0.13, F = O = −1.33, Cl = O = −0.02, Total = 99.33. Normalized to 3 (P+S) and 1 (OH,F,Cl) *p.f.u.*, this composition yields the formula $(Na_{0.005}Ca_{4.985}La_{0.003}Ce_{0.003}Nd_{0.002})(P_{2.971}S_{0.029})O_{12.014}[F_{0.845}Cl_{0.011}(OH)_{0.144}]$.

5. Crystal Morphology

The crystal morphology of fluorapophyllite-(K) from Aleului Valley was described by [10]. In the definition of crystallographic forms, Ref. [10] used the crystallographic orientation conducted by [34], describing a combination of basal pinacoids {001}, prisms {100}, and low pyramids {111}. As shown by [35,36], this orientation must be reconsidered, but the combination of faces remains the same. The mineral occurs as crystals tabular on [001], up to 1 cm across and 1 mm thick. The (001) faces exhibit relatively rough surfaces, lacking any sign of growth steps.

Transversal sections of typical crystals of the mineral are given in Figure 4, whereas Figure 5 shows a typical aggregate of crystals. The individual crystals have a simple combination of forms consisting of basal pinacoids {001}, prisms {110}, and low pyramids {101}. Transversal sections, as well as geometrical goniometry on isolated crystals, allowed the exact measurement of angles between prism and pyramid faces. A similar combination of crystal faces was depicted for fluorapophyllite-(K) by [35,36]. No twinning was identified. The perfect cleavage parallel to (001) is clearly visible.

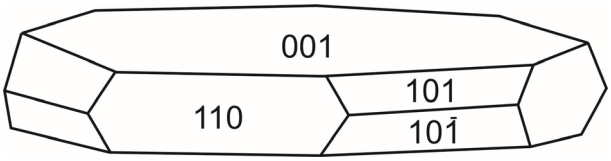

Figure 4. Sketch of a fluorapophyllite-(K) crystal showing the crystal form, consisting of a combination of basal pinacoids (001), low pyramid faces (101), and (110) prisms.

Figure 5. Micromount of fluorapophyllite-(K), showing a stack of tabular crystals with forms depicted in Figure 4.

6. Chemical Data

Electron-microprobe analyses of nine representative samples of fluorapophyllite-(K) from Valea Rea are given in Table 1. Each analysis represents the average of N points of analysis across the same crystal or group of crystals from a thin section. No chemical zoning or inhomogeneity was observed across the same crystal. As nitrogen was not measured by EMPA, the analyses in Table 1 were calculated on a cationic basis [i.e., 8 (Si+Al)], as

already conducted by [37,38] and accepting that the cations in tetrahedral coordination were the most stable under the electron beam. Water in hydroxyl was calculated for the charge balance, whereas the molecular water was calculated to reach the stoichiometry.

Table 1. Representative electron-microprobe analyses of fluorapophyllite-(K), Aleului Valley *.

Sample	212a	212b	212c	212d	212e	213a	213b	213c	213d	Mean
N [1]	9	9	7	9	10	8	7	10	8	77
SiO_2	51.24	51.43	51.17	51.45	51.35	52.39	51.9	51.22	51.49	51.50
Al_2O_3	0.39	0.31	0.32	0.30	0.30	0.00	0.21	0.26	0.24	0.26
CaO	24.23	24.32	24.17	24.22	24.20	24.33	24.43	24.14	24.11	24.23
MnO	0.01	0.01	0.01	0.00	0.01	0.01	0.01	0.00	0.01	0.01
FeO [2]	0.02	0.03	0.03	0.02	0.02	0.02	0.01	0.01	0.01	0.02
MgO	0.00	0.01	0.01	0.01	0.01	0.01	0.00	0.01	0.01	0.01
BaO	0.01	0.02	0.01	0.03	0.02	0.01	0.00	0.01	0.02	0.01
SrO	0.01	0.01	0.00	0.00	0.00	0.00	0.00	0.00	0.00	0.00
K_2O	5.00	5.03	4.99	4.99	5.00	5.07	4.97	4.99	4.98	5.00
Na_2O	0.05	0.04	0.04	0.02	0.04	0.02	0.03	0.04	0.04	0.04
F	2.17	1.54	2.02	2.20	1.90	1.57	1.62	2.04	1.39	1.84
Cl	0.00	0.00	0.01	0.00	0.01	0.00	0.00	0.01	0.01	0.00
H_2O [3]	16.07	15.76	15.94	16.13	15.94	15.99	15.94	15.94	15.75	15.94
O = F	−0.92	−0.65	−0.85	−0.93	−0.80	−0.66	−0.68	−0.86	−0.59	−0.78
O = Cl	−0.00	−0.00	−0.00	−0.00	−0.00	−0.00	−0.00	−0.00	−0.00	−0.00
Total	98.28	97.86	97.87	98.44	98.00	98.76	98.43	97.81	97.48	98.09
Number of cations on the basis of 8 (Si + Al)										
Si	7.929	7.944	7.941	7.945	7.945	8.000	7.962	7.952	7.956	7.952
Al	0.071	0.056	0.059	0.055	0.055	0.000	0.038	0.048	0.044	0.048
Ca	4.017	4.025	4.019	4.007	4.012	3.981	4.015	4.016	3.992	4.010
Mn	0.001	0.001	0.001	0.000	0.001	0.001	0.001	0.000	0.001	0.001
Fe^{2+}	0.003	0.004	0.004	0.003	0.003	0.003	0.001	0.001	0.001	0.003
Mg	0.000	0.002	0.002	0.002	0.002	0.002	0.000	0.002	0.002	0.002
Ba	0.001	0.001	0.001	0.002	0.001	0.001	0.000	0.001	0.001	0.001
Sr	0.001	0.001	0.000	0.000	0.000	0.000	0.000	0.000	0.000	0.000
K	0.987	0.991	0.988	0.983	0.987	0.988	0.973	0.988	0.982	0.986
Na	0.015	0.012	0.012	0.006	0.012	0.006	0.009	0.012	0.012	0.011
F	1.062	0.752	0.991	1.074	0.930	0.758	0.786	1.002	0.679	0.899
Cl	0.000	0.000	0.003	0.000	0.003	0.000	0.000	0.003	0.003	0.001
$(OH)^-$ [3]	0.585	0.237	0.499	0.612	0.451	0.288	0.308	0.513	0.238	0.421
H_2O	8.000	8.000	8.000	8.000	8.000	8.000	8.000	8.000	8.000	8.000
Composition in end members (mol.%)										
F-Apo-(K)	64.48	76.04	66.51	63.70	67.34	72.47	71.85	66.14	74.05	68.11
(OH)-Apo-(K)	35.52	23.96	33.49	36.30	32.66	27.53	28.15	33.86	25.95	31.89

* Results expressed in wt.%; [1] number of point analyses; [2] total iron as FeO; [3] as calculated.

A few remarks must be drawn based on the results in Table 1, as follows:

(1) Even partially, the analyses in Table 1 show that fluorine prevails over hydroxyl, defining fluorapophyllite-(K) with only 23.96 to 36.30 mol.% (mean 31.89 mol.%) hydroxyapophyllite-(K) in a solid solution. Note that all but 4 from the 77 point analyses define fluorapophyllite-(K), with the remaining 4 points defining hydroxyapophyllite-(K).

(2) Cs was sought but not detected, so the isomorphism toward fluorapophyllite-(Cs) cannot be considered.

(3) The measurements for Sr gave very low contents (up to 0.01 wt.% SrO), and the hydroxymcglassonite-(K) substitution is also negligible. Generally, the Sr contents are lower than those of Ba (Table 1).

(4) The Al-for-Si substitution is not important, as found for example by [39]: Only up to 0.9% of the [4]-coordinated Si sites are occupied by Al.
(5) The replacement of K by Na is generally low (0.6 to 1.5% of the K positions are occupied by Na), confirming the pseudo-solid solution between fluorapophyllite-(K) and fluorapophyllite-(Na).

In contrast, the tests for ammonia showed that the ammonium ion is present as a substitute for K^+. A bulk chemical analysis on a separate aliquot gave NH_3 = 0.14 wt.%, which corresponds to 0.20 wt.% $(NH_4)_2O$. A complete analysis is, therefore, (in wt.%) SiO_2 = 51.50, Al_2O_3 = 0.26, CaO = 24.23, MnO = 0.01, FeO = 0.02, MgO = 0.01, BaO = 0.01, K_2O = 5.00, Na_2O = 0.04, $(NH_4)_2O$ = 0.20, H_2O = 16.04, F = 1.84, F = O = −0.78, Total = 98.38. Water was calculated based on the total weight loss recorded on the thermogravimetric curve, by subtracting ammonia. The chemical-structural formula, calculated on the basis of 8(Si+Al) and 1(OH+F), is $[K_{0.985}Na_{0.012}(NH_4)_{0.076}]_{\Sigma=1.073}$ $(Ca_{4.009}Mn_{0.001}Fe^{2+}{}_{0.003}Mg_{0.002}Ba_{0.001})_{\Sigma=4.016}$ $(Si_{7.953}Al_{0.047})O_{20.029}[F_{0.899}(OH)_{0.101}]\cdot 8.059H_2O$.

The basis for calculation was preferred over 29(O,OH,F), e.g., [7,11,39–41], or 13 cations, 21(O), and 1 (OH+F) [9]. The formula defines ammonium-bearing fluorapophyllite-(K) with 7.08% $(NH_4)^+$ and 1.12% Na at the A sites, normally occupied by K. The percentage of hydroxyapophyllite-(K) in the solid solution is only 10.1 mol.%. Both the A and B sites in the structure (see below) are slightly overcompensated, and water in excess may be due to the adsorbed water.

7. Structure

The structure study of the members of the fluorapophyllite-(K)—hydroxyapophyllite-(K) solid-solution series, of *P*4/*mnc* symmetry, is of considerable interest. After the pioneering work of [42], the fluorapophyllite-(K) structure was refined by [40,43–48] whereas that of hydroxyapophyllite-(K) was solved by [37,49]. The structural refinements of both fluorapophyllite-(Cs) [2] and fluorapophyllite-(NH_4) [3] were performed in the same space group, as well as the refinement of hydroxymcglassonite-(K) [4]. Fluorapophyllite-(Na) is orthorhombic, space group *Pnnm* [6,50].

The structural refinement of a representative sample of fluorapophyllite-K from Aleului Valley (Sample 213) was performed in order to supplement the data on the mineral. The structure was refined in space group *P*4/*mnc*. The structure was refined to R = 0.026 as compared with R = 0.037 [44] or R = 0.035 [37] or [46]. The details of the data collection and refinement are provided in Table 2. All atoms besides hydrogen atoms were refined with anisotropic thermal parameters, and those parameters, as well as the atoms' coordinates, are provided in Tables 3–6. Free refinement of the occupancy factors of the cation sites indicated that they are fully occupied. The occupancy of the OH/F site has been constrained to 0.768 F + 0.232 O, in agreement with the electron microprobe chemical data. The bond distances and bond-valence sums are given in Tables 3–6.

Table 2. Details of the X-ray data collection and refinements of fluorapophyllite-(K).

Crystal Data	
Crystal shape	Plate
Color	colorless
Crystal size (mm)	0.39 × 0.20 × 0.02
Temperature (K)	293(2)
a (Å)	8.9685(1)
c (Å)	15.7885(5)
V (Å^3)	1269.93(4)
Space group	*P*4/*mnc*
Z	2
$D_{calc.}$ (g/cm^3)	2.371

Table 2. *Cont.*

Data collection	
Diffractometer	Rigaku Xcalibur, CCD Detector
Radiation; λ	MoK_α; 0.71073
Absorption coefficient (mm^{-1})	1.521
$F(000)$	920
Max. 2θ (°)	64.88
Range of indices	$-7 < h < 13$ $-12 < k < 13$ $-23 < l < 22$
Number of measured reflections	12,521
Number of unique reflections	1157/948
Criterion for observed reflections	$I > 3\sigma(I)$
Refinement	
Refinement on	Full-matrix least squares on F^2
Number of refined parameters	52
$R_1(F)$ with $F_0 > 4s(F_0)$ *	0.0258
$R_1(F)$ for all the unique reflections *	0.0871
$wR_2(F^2)$ *	0.0377
R_{int} (%)	0.0952
S ("goodness of fit")	1.00
Weighing scheme	$1/(\sigma^2(I)^2) + 0.0049(I)^2$
Min./max. residual e density, (eÅ^{-3})	−0.55, 0.65

* Notes: $R_1 = \Sigma(|Fobs| - |Fcalc|)/\Sigma|Fobs|$; $wR_2 = \{\Sigma[w(F^2obs - F^2calc)^2]/\Sigma[w(F^2obs)^2]\}^{1/2}$. $W = 1/[s^2(F_0{}^2) + (aP)^2 + bP]$, where $P = [2F_c{}^2 + Max(F_0{}^2,0)]/3$, where a, b are shown in the refinement process.

Table 3. Atom coordinates and anisotropic displacement parameters (Å^2) for fluorapophyllite-(K).

	x	y	z	U_{eq}
Ca	0.11003(5)	0.24597(5)	0	0.0090(1)
K	0	0	0.5	0.0317(4)
Si	0.22625(5)	0.08627(5)	0.18992(3)	0.0066(1)
O1	0.8637(1)	0.3637(1)	0.25	0.0097(3)
O2	0.0846(1)	0.1896(1)	0.21773(9)	0.0133(3)
O3	0.2646(1)	0.1016(1)	0.09217(8)	0.0119(3)
O4	0.2140(1)	0.4486(2)	0.08984(8)	0.0225(4)
F/OH *	0	0	0	0.0152(7)
H1	0.175953	0.531738	0.089111	0.027
H2	0.28644	0.432341	0.120183	0.027

* Refined with the occupancy 0.768 F + 0.232 O.

Table 4. Anisotropic displacement parameters (Å^2) for fluorapophyllite-(K).

	U_{11}	U_{22}	U_{33}	U_{12}	U_{13}	U_{23}
Ca	0.0087(2)	0.0095(2)	0.0090(2)	0.0006(1)	0	0
K	0.0233(4)	0.0233(4)	0.0485(9)	0	0	0
Si	0.0062(2)	0.0065(2)	0.0072(2)	−0.0003(1)	−0.0012(1)	−0.0006(1)
O1	0.0093(5)	0.0093(5)	0.0105(8)	0.0003(6)	0.0018(4)	−0.0018(4)
O2	0.0085(5)	0.0142(6)	0.0173(7)	0.0031(4)	−0.0014(5)	−0.0034(5)
O3	0.0132(6)	0.0142(6)	0.0084(6)	0.0008(4)	−0.0008(5)	−0.0006(5)
O4	0.0341(9)	0.0149(6)	0.0185(8)	0.0012(6)	−0.0034(6)	−0.0044(6)
F/OH	0.0092(8)	0.0092(8)	0.027(2)	0	0	0

Table 5. Bond distances (Å) observed in the crystal structure of fluorapophyllite-(K).

K-O4 x8	2.967(1)	Si-O1	1.619(1)
		Si-O2	1.628(1)
Ca-O3 x2	2.391(1)	Si-O2	1.633(1)

Table 5. *Cont.*

Ca-O3 x2	2.397(1)	Si-O3	1.587(1)
Ca-O4 x2	2.487(1)	<Si-O>	1.617
Ca-F/OH	2.417(1)		
<Ca-ϕ>	2.424		
Bond	O-H (Å)	H···O (Å)	O-H···O (°)
O4-H1···O3	0.82(1)	1.945(1)	174.9(1)
O4-H2···O2	0.82(1)	2.572(1)	131.1(1)

ϕ = O^{2-} or F^{-}.

Table 6. Detailed bond-valence table (*vu*) for the crystal structure of fluorapophyllite-(K) *.

	K	Ca	Si	H1	H2	Σ
O1			1.014 × 2→			2.03
O2			0.989 0.976		0.119	2.08
O3		0.318 × 2↓ 0.313 × 2↓	1.105	0.231		1.97
O4	0.105 × 8↓	0.245 × 2↓		0.766	0.766	1.88
F/OH		0.211 × 4→				0.85
Σ	0.84	1.96	4.08	1.00	0.88	

* Bond-valence parameters are from [51], except [52] for Si–O.

In the resolved structure, the four- and eight-membered rings of SiO_4 tetrahedra form a $(Si_8O_{20})^{8-}$ sheet, perpendicular to [001]. The $(Si_8O_{20})^{8-}$ sheets connect via cations: K (A site) and Ca (B site), as well as via hydrogen bonding (Figure 6a,b). The A cation is coordinated by eight H_2O groups, and the B cation is coordinated by four O anions of SiO_4 tetrahedra, two H_2O groups, and F (Figure 6, bottom). Part of the water molecules are replaced by $(OH)^{-}$ anions, with the remaining proton bonded to fluorine to form HF molecules [44], giving, in our case, the ideal structural formula of $KCa_4(Si_4O_{10})[(HF)_{0.768}(OH)_{0.232}]\cdot 7.232H_2O(OH)_{0.768}$. The obtained structure is better depicted in Figure 6. Figure 6 (bottom) clearly shows that K^+ is coordinated by eight water O atoms and Ca is coordinated by four silica-layer O ions, two water O ions, and F^{-}, as described by [11].

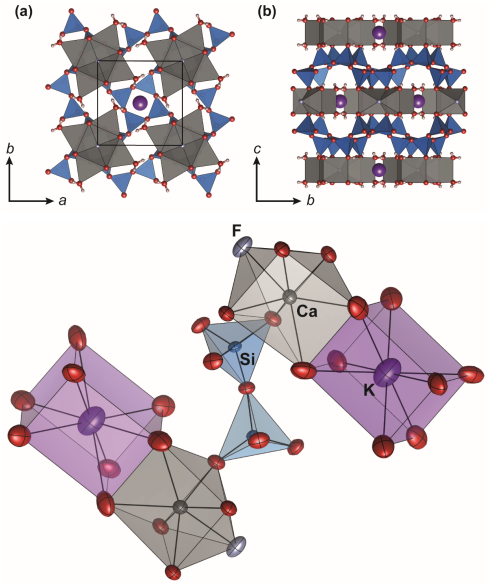

Figure 6. Crystal structure of fluorapophyllite-(K). Top: Projection along the *c*- ((**a**)—**left**) and *a*-axes ((**b**)—**right**) of the structure. Blue and gray polyhedra represent SiO_4 and CaO_7, respectively. Potassium atoms are represented as purple, oxygen atoms as red, fluorine atoms as light blue, and

hydrogen atoms as white balls. The quadrangle in the left figure represents one unit-cell. **Bottom**: Detailed view of the coordination between KO_8, CaO_6F, and SiO_4 polyhedra in the structure of fluorapophyllite-(K). Hydrogen atoms were omitted for clarity. The displacement ellipsoids represent the 90% probability level.

8. X-ray Data

Cell parameters of two selected samples were successfully refined by least squares, based on a tetragonal *P*4/*mnc* cell, after indexing the patterns on the basis of structural data, which closely fit with PDF 19-0944. Eighty reflections in the 2θ range between 10 and 90°, for which unambiguous indexing was possible, were used for refinement. The obtained cell parameters are a = 8.987(1) Å and c = 15.805(3) Å for Sample 212 and a = 8.976(2) Å and c = 15.783(4) Å for Sample 213, respectively. In both cases, the values are relatively close to that determined by single-crystal X-ray diffraction (Table 2) and in the range of values obtained for hydroxy- and fluorapophyllite-(K) by various authors (Table 7).

Table 7. Unit-cell parameters of tetragonal (*P*4/*mnc*) minerals in fluorapophyllite-(K)—hydroxyapophyllite-(K) solid-solution series from various occurrences.

Mineral Species	Sample Origin	Host Rock	Reference	a (Å)	c (Å)
fluorapophyllite-(K)	Phoenix Mine, Michigan, USA	basalt	[40]	8.963(2)	15.804(2)
fluorapophyllite-(K)	Phoenix Mine, Michigan, USA	basalt	[40]	8.965(2)	15.768(2)
fluorapophyllite-(K)	Mont St. Hillaire, Quebec, Canada	basalt	[43]	8.965(3)	15.767(7)
fluorapophyllite-(K)	Poona, India	basalt	[53]	8.965(3)	15.756(7)
hydroxyapophyllite-(K)	Ore Knob, Jefferson, NC, USA	sulfide ore	[37]	8.978(3)	15.83(1)
hydroxyapophyllite-(K)	Kimberley, South Africa	kimberlite	[49]	8.979(4)	15.83(1)
hydroxyapophyllite-(K)	Mofjellet mine, Rana, Norway	mica gneiss	[38]	8.968(0)	15.869(13)
fluorapophyllite-(K)	Andersberg, Germany	basalt	[46]	8.966(2)	15.767(1)
fluorapophyllite-(K)	Nasik, India	basalt	[47]	8.970(1)	15.792(4)
fluorapophyllite-(K)	Blomindon, Nova Scotia, Canada	basalt	[54]	8.969(1)	15.796(2)
hydroxyapophyllite-(K)	Giken Mine, Sulitelma, Norway	sulfide ore	[54]	8.985(2)	15.875(3)
hydroxyapophyllite-(K)	Aleului Valley, Pietroasa, Romania	skarn	[10]	8.973(1)	15.769(2)
fluorapophyllite-(K)	Międzyrzecze, Poland	skarn	[11]	8.974(2)	15.798(6)
fluorapophyllite-(K)	Trabzon, Turkey	basalt	[41]	8.978	15.830
hydroxyapophyllite-(K)	unknown	unknown	[55]	8.9345(6)	15.9831(7)
fluorapophyllite-(K)	unknown	unknown	[56]	8.954(2)	15.795(2)
fluorapophyllite-(K)	Aleului Valley, Pietroasa, Romania	skarn	present study (S 212)	8.987(1)	15.805(3)
fluorapophyllite-(K)	Aleului Valley, Pietroasa, Romania	skarn	present study (S 213)	8.976(2)	15.783(4)

The observed and calculated reflections are given as supplementary materials, in Tables S2 and S3, respectively. The slightly larger values of cell parameters as compared with those refined for fluorapophyllite-(K) and reported in Table 7 are due both to the $(OH)^-$-for-F^- and $(NH_4)^+$-for-K^+ substitutions. In fact, the second substitution plays a major role in the "expansion" of the unit cell, because of the larger ionic radii of the eight-fold coordinated $(NH_4)^+$ as compared with the eight-fold coordinated K^+ (1.54 Å vs. 1.51 Å, respectively, according to [57] and [58], respectively). This trend is clearly visible in the case of the unit-cell parameters of fluorapophyllite-(NH_4), i.e., a = 8.99336(9) Å and c = 15.7910(3) Å [3].

9. Physical Properties

Fluorapophyllite-(K) from Aleului Valley skarns occurs as translucent, clear, colorless to turbid white (toward the rim) crystals. The mineral is luminescent both under long-wave (366 nm) and short-wave (254 nm) ultraviolet radiation, with the luminescence tints being yellowish-white and greenish-yellow, respectively.

The mineral is uniaxial positive. The indices of refraction, each taken as the mean of ten measurements on different grains, are ω = 1.534(1) and ε = 1.536(1), lower than those measured for hydroxyapophyllite-(K) [37] or for fluorapophyllite-(NH_4) [3]. This confirms the paucity of (OH)-for-F and (NH_4)-for-K substitutions, which normally result in increasing refraction indices. The mean refraction index, calculated as $\overline{n} = (2\omega + \varepsilon)/3$ [59], is 1.535.

The mean measured density, taken as the average of measurements on 10 different grains, is D_m = 2.379(4) g/cm^3, which compares well with the calculated density, obtained on the basis of chemical data given before and of the unit cell volume in Table 2, for Z = 2 formula units per cell [42], i.e., D_x = 2.381 g/cm^3.

As derived from the mean refractive index given before and from the measured density, the physical refractive energy is K_p = 0.2249. The chemical refractive energy (K_C) value, based on the formula given before and on the constants of [60], is K_c = 0.2265. The calculation of the Gladstone–Dale compatibility index ($1 - K_p/K_c$) yielded a value of 0.007, indicative of superior agreement between physical and chemical data [60]. The physical refractive energy calculated on the basis of the calculated value of density is K_p = 0.2247. The use of this value in the calculation does not substantially influence the compatibility index, which is 0.008 and remains "superior" as ranked by [60].

10. Thermal Behavior

Investigations of the thermal behavior of fluorapophyllite-(K) and of related end-members of the group were carried out by quite a large number of authors (e.g., [11,38,43,45,47,54,61–63]). The DTA and TG curves recorded for fluorapophyllite-(K) from Aleului Valley using the analytical conditions given in Chapter 3 are given in Figure 7.

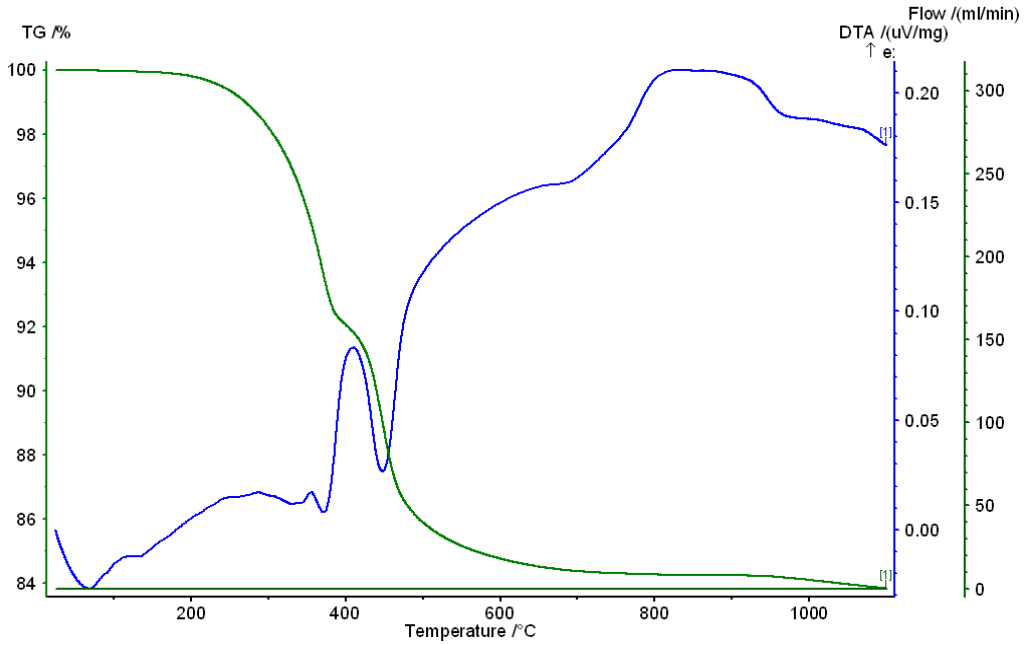

Figure 7. Thermal curves recorded for a representative sample of fluorapophyllite-(K) from Aleului Valley: Differential thermal analysis (blue) and thermogravimetric analysis (green).

The DTA curve shows four endothermic peaks centered at 330 °C, 371 °C, 448° C, and 634 °C, respectively, and an exothermic effect, centered at 833 °C, with a shoulder

toward lower temperatures. Two weak endothermic effects recorded at lower temperatures (81 °C and 121 °C) are due to the loss of adsorbed and fluid-inclusion water, respectively, from the (ground) sample. The first three endothermic effects, observed in fluorapophyllite by the majority of authors, e.g., [11,38,43,45,47,62,63], are due to dehydration and may be interpreted as follows:

(1) The effect at 330 °C, which has a small shoulder toward low temperatures and is associated with a weight loss of 6.01 wt.%, corresponds to the removal of 1 molecule *p.f.u.* of the weakly bounded water [47]. The XRD analysis of the cooled product shows the persistence of an apophyllite-type structure, as observed by [47] for the "partially dehydrated fluorapophyllite".

(2) The effect at 371 °C, associated with a loss-in-weight of 4.99 wt.%, seems to correspond to the removal of three other water molecules *p.f.u.* [47] and to the structural breakdown. The resulting product is amorphous.

(3) The third effect, at 448 °C, marks the loss of the remaining water coupled with the dehydroxylation. It corresponds to a loss-in-weight of 5.25 wt.%. The resulting product is still amorphous. The first and third exothermal effects were both recorded in the range of temperatures reported by [54] as characteristic of fluorapophyllite terms: 310–334 °C and 430–450 °C, respectively.

(4) The fourth effect, recorded at 634 °C, is due to the depletion of NH_3. The loss-in-weight recorded on the TGA curve is irrelevant since the process is combined with the oxidation of ammonia. The total weight loss is 16.24 wt.%.

The exothermal effect, recorded on the DTA curve at 833 °C, expresses the recrystallization of a breakdown product.

11. Infrared and Raman Behavior

Considerable interest was devoted to the study of both infrared ([3,8,11,40,54,63–67]) and Raman ([3,11,65,66,68–70]) factors of fluorapophyllite-(K). Therefore, the attribution of the bands in the spectra in Figures 8 and 9, which depict representative FTIR and Raman spectra, respectively, was considerably facilitated and is attempted in Table 8.

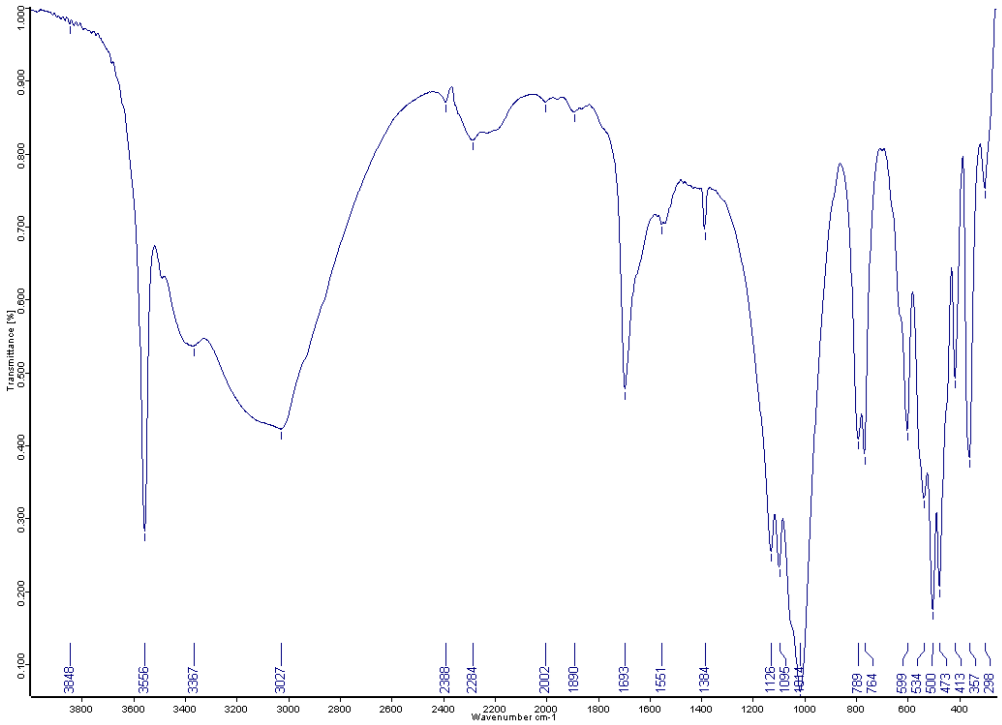

Figure 8. FTIR spectrum of a representative sample of fluorapophyllite-(K) from Aleului Valley.

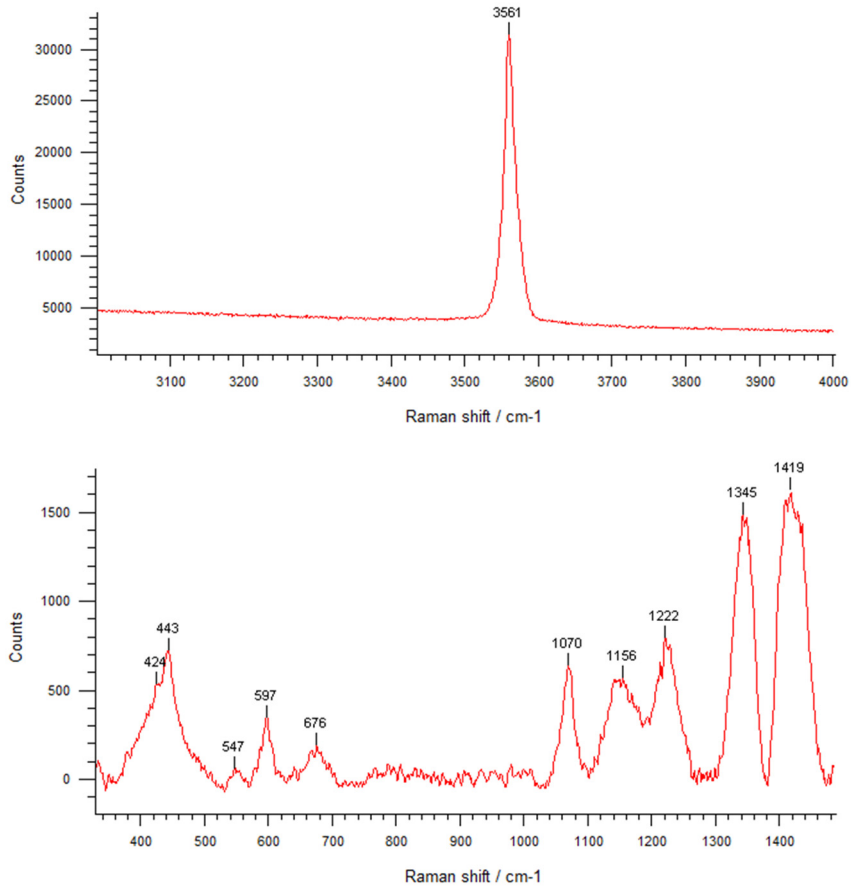

Figure 9. Raman spectrum of a representative sample of fluorapophyllite-(K) from Aleului Valley as recorded in the high (**top**) and low-to-medium (**bottom**) shift regions.

Table 8. Positions and assignments of the FTIR and Raman bands recorded for selected samples of ammonium-bearing fluorapophyllite-(K) from Valea Aleului [1].

Structural Group	Vibrational Mode	Wavenumber (cm^{-1})			Character, Intensity [2]
		FTIR		Raman	
H_2O	H-O-H stretching	3566	3566	3561	s, sh
H_2O, $(NH_4)^+$	H-N-H stretching, 3 γ (OH) overtone	3367	3369	-	m, b
H_2O	H-O-H stretching	3027	3028	-	s, b
H_2O	2 δ (OH) overtone	2386	2387	-	w, b
H_2O	2 γ (OH) overtone	2284	2285	-	w, b
H_2O	H-O-H "scissors" bending	1693	1694	-	m, sh
H_2O	H-O-H "scissors" bending	1683	1680	-	m, shd
H_2O	H-O-H bending	1551	1549	-	w, b
$(NH_4)^+$	H-N-H in plane bending	1384	1384	1419 1345	w, sh
$(OH)^-$	δ (H-O-H) (in plane) bending	1192	1193	-	m, shd
$(SiO_4)^{4-}$, $(OH)^-$	ν_3 antisymmetric stretching, γ (OH)	1126	1127	1156	s, sh

Table 8. *Cont.*

Structural Group	Vibrational Mode	Wavenumber (cm^{-1})			Character, Intensity [2]
		FTIR		Raman	
$(SiO_4)^{4-}$	ν_1 symmetric stretching	1095	1096	1070	s, sh
$(SiO_4)^{4-}$	$\nu_{3'}$ antisymmetric stretching	1051	1050		vs, shd
$(SiO_4)^{4-}$	$\nu_{3''}$ antisymmetric stretching	1014	1014		vs, sh
H_2O	H-O-H (water) libration	988	989	849	s, shd
$(SiO_4)^{4-}$	ν_2 out-of-plane bending (O-Si-O)	789	788		m, sh
		764	764		m, sh
$(SiO_4)^{4-}$	ν_4 in-plane bending (O-Si-O)	599	600	597	m, sh
$(SiO_4)^{4-}$	$\nu_{4'}$ in-plane bending (O-Si-O)	534	535	546	s, sh
$(SiO_4)^{4-}$	$\nu_{2'}$ out-of-plane bending (O-Si-O)	500	500	486	vs, sh
$(SiO_4)^{4-}$	$\nu_{4''}$ in-plane bending (O-Si-O)	473	474	443	vs, sh
		413	412	424	m, sh
				401	
		357	357	339	m, sh
	lattice vibrations (?)	298	291		w, sh
		265	266	232	w, shd
		-	-	166	
		-	-	140	
		-	-	108	

[1] Assumptions according to the authors referred to in the text; [2] character of the bands on the FTIR spectrum: s = strong; m = medium; w = weak; vs = very strong; sh = sharp; b = broad; shd = shoulder.

The analysis of FTIR and Raman spectra reveals some particularities, as follows:

(1) There are three bands clearly recognizable on the infrared spectra in the OH-stretching region between 3000 and 4000 cm^{-1}, in perfect agreement with the structure determination (see before). Two hydrogen bonds imply the water molecules in the structure, generating two absorption bands in the theoretical range of 2838–3663 cm^{-1} [71]. According to the bond distance–frequency correlation equation of [71], the nominal frequencies of these bands must occur, for OH...O distances of 2.765 and 3.392 Å issued from the structure refinement but calculated for O-H-O angles of 180°, at 3345 and 3590 cm^{-1}, respectively. The two bands in the spectrum in Figure 8 specifically occurring at 3367 and 3566 cm^{-1}, respectively, could be consequently assumed to be the OH-stretching vibrations involving hydrogen-bonded water molecules. In the Raman spectrum, a band located at 3561 cm^{-1} (Figure 9, top) materializes the OH stretching. Its presence was considered indicative for the hydroxyl-bearing apophyllite-group minerals [70]. The presence of a sole band on the Raman spectrum (i.e., that at 3561 cm^{-1}) is, on the other hand, characteristic of fluorapophyllite-(K) [68].

(2) The broad absorption band recorded at ~3030 cm^{-1} in the infrared spectrum, assumed by [40] to be a water stretch, seems to be due to an ammonium stretch vibration combined with an OH stretch, and expresses a third hydrogen bond.

(3) Bands at ~2385 and 2285 cm^{-1} were also observed on the infrared spectra of fluor- and hydroxyapophyllite-(K) (e.g., [8,64,66]) and correctly assumed to (OH) modes. As in most of the compounds with asymmetric hydrogen bridges [64,72], these bands must represent overtones of the OH-bending modes. Judging by their spectral position and shape, the medium-to-strong absorption band at ~1125 cm^{-1} could be assigned to the bending motion γ (OH) (out-of-plane) of the Si-OH bond. The 3 γ (OH) and 2 γ (OH) overtones must consequently occur near the values recorded for the bands at ~3365 cm^{-1} and ~2285 cm^{-1}, respectively. The other (OH) bending, δ (in-plane), must be expressed by a band expressed like a shoulder, at ~1190 cm^{-1}, with the band at ~2385 cm^{-1} representing its second-rank overtone.

(4) The presence of two distinct H_2O sites, as indicated by the results of the crystal structure analysis (see before), explains the pronounced splitting of the H-O-H bending motions of molecular water: The bending at ~1695 cm^{-1}, expressed by a sharp band with a visible shoulder at ~1680 cm^{-1}, and the broad and weak band centered at ~1545 cm^{-1}. The shouldered band at ~1695 cm^{-1} could be assumed to be strongly hydrogen-bonded water molecules, whereas the band at ~1640 cm^{-1} is due to weakly hydrogen-bonded water.

(5) The weak but sharp absorption band at ~1385 cm^{-1} is due to the ammonium ion (e.g., [73]), which was detected in ammonium-bearing fluorapophyllite-(K) (i.e., [3,54]) and expresses its in-plane bending mode. The band is double degenerate on the Raman spectrum (Table 8).

(6) The bands in the range of 1100–900 cm^{-1} could be assigned to the stretching of silicate groups in the structure. The corresponding modes, including the bending vibrations, active in both Raman and infrared, are depicted in Table 8 and correspond to the assumptions of [11,68]. The silicate anion seems to have 9 vibrational modes, namely $1\nu_1 + 3\nu_3 + 2\nu_2 + 3\nu_4$. If the assignments in Table 8 are correct, and none of the quoted absorption bands are due to lattice vibrations, this band multiplicity is consistent with a C_δ punctual symmetry of the (distorted) silicate anion, which agrees with the structure described before.

12. Genetic Considerations

The crystallization of fluorapophyllite-(K) from Aleului Valley is an expression of the late hydrothermal activity associated with the intrusion of Pietroasa pluton. Textural and chemical particularities indicate that the mineral formed at a late hydrothermal magmatic stage, postdating talc, and it crystallized from a volatile F-rich and low-viscosity fluid phase, which can also accommodate ammonium. Genesis at relatively low temperatures, i.e., 250–350° as estimated by [11], is supported by the co-crystallization with pectolite. During the first, prograde evolution of the host endoskarn, a paragenesis consisting of wollastonite + K-feldspar + diopside defines the peak thermal conditions. The exoskarn is magnesian, defined by a peak association consisting of forsterite + spinel [10]. Resumed to the endoskarn zone, subsequent retrogressive reactions induced by F-rich, aqueous fluids from the magmatic source conduce to the formation of talc on diopside and the crystallization of fluorapatite. Later-stage fluids have essentially the same composition and conduce to the crystallization of fluorapophyllite-(K). The source for K and Ca is the feldspar, whereas F is expelled by the magmatic body. Pectolite, intergrown with fluorapophyllite-(K), fixes the Na in excess, as a solid solution between fluorapophyllite-(K) and fluorapophyllite-(Na) could not be imagined, due to the differences in structure and symmetry between the two mineral species (see before).

13. Conclusions

Ammonium-bearing fluorapophyllite-(K) from Aleului Valley endoskarn was formed during a low-temperature retrograde stage of the skarn system evolution when late F-bearing affected the pre-existing mineral parageneses. The late fluorinate solutions could easily accommodate ammonium, resulting in an ideal structural formula for the mineral of $[K_x(NH_4)_{1-x}]Ca_4(Si_8O_{20})[F_y(OH)_{1-y}]\cdot 8H_2O$ type. In fact, almost all the terms defined as

fluorapophyllite-(K) contain low amounts of ammonium as a substitute for K^+ (e.g., [54,67]). Apparently, the presence of NH_4F in solution accelerates the crystallization and decreases the number of crystal defects, as in the case of zeolites [74].

In spite of the difference in the ionic radii between the eight-fold coordinated $(NH_4)^+$ and the eight-fold coordinated K^+, the presence of small amounts of ammonium as a substitute for K^+ does not substantially affect the fluorapophyllite-(K) structure, as it was determined by refinement based on X-ray diffraction, a phenomenon already observed [67]. The small amounts of lower ionic radii Na^+ that also substitute for K^+ could explain this behavior.

On the other hand, the presence of ammonium in the mineral structure explains the decomposition in four steps observed in the differential thermal analysis, as already mentioned [63]. The analysis of data from vibrational spectroscopy provided support for the high symmetry in the *P*4/*mnc* space group, in spite of the reduction in the symmetry of SiO_4^{4-} ion from T_d to C_δ.

Supplementary Materials: The following supporting information can be downloaded at: https://www.mdpi.com/article/10.3390/min13111362/s1, Table S1: Representative electron-microprobe analyses of pectolite, Aleului Valley; Table S2: X-ray powder data of a selected sample of fluorapophyllite-(K) from Aleului Valley: Sample 212; Table S3: X-ray powder data of a selected sample of fluorapophyllite-(K) from Aleului Valley: Sample 213.

Author Contributions: Conceptualization, Ş.M., D.-G.D., C.S.G., F.H. and F.D.B.; formal analysis, Ş.M., C.S.G., A.E.F., G.C. and F.D.B.; funding acquisition, Ş.M., C.S.G. and F.D.B.; investigation, Ş.M., D.-G.D., A.E.F. and F.D.B.; methodology, Ş.M., D.-G.D. and F.D.B.; resources, Ş.M., D.-G.D. and C.S.G.; data curation, D.-G.D., C.S.G., G.C. and F.D.B.; writing—original draft preparation, Ş.M.; writing—review and editing, Ş.M.; visualization, Ş.M.; supervision, Ş.M.; project administration, Ş.M., D.-G.D., C.S.G. and F.D.B. All authors have read and agreed to the published version of the manuscript.

Funding: This study was partly supported by a scientific cooperative research grant awarded by the Walloon and Romanian Governments (4 BM/2021). Other grants awarded to the authors by UEFISCDI in Romania (PN-III-P1-1.2-PCCDI-2017-0346 and PN-III-P1-1.1-MC-2018-3163) and by the Ministry of Research, Innovation, and Digitization (PN23-39-02-01/2023, PN23-39-02-06/2023 and PN23-39-02-07/2023) generously supported the final draft.

Data Availability Statement: The data presented in this study are available on request from the corresponding author. The data are not publicly available due to the differences in the national politics regarding data availability.

Acknowledgments: The use of the EPMA facility at the Department of Earth, Environmental, and Planetary Sciences, Rice University, Houston, Texas, is kindly acknowledged. The assistance of George Dincă in the Raman spectrometry work, of Erna Călinescu ("Prospecţiuni" S.A., Bucharest) in the wet-chemical analysis, and of Adrian Iulian Pantia (Geological Institute of Romania, Bucharest) in the X-ray powder and thermal analyses are gratefully acknowledged. Fruitful discussions on the field with the late Jean Verkaeren and with Bernard Guy, Essaïd Bilal, Gheorghe Ilinca, André-Mathieu Fransolet, and Maxime Baijot were highly appreciated.

Conflicts of Interest: The authors declare no conflict of interest.

References

1. Hatert, F.; Mills, S.J.; Pasero, M.; Williams, P.A. CNMNC guidelines for the use of suffixes and prefixes in mineral nomenclature, and for the preservation of historical names. *Eur. J. Mineral.* **2013**, *25*, 113–115. [CrossRef]
2. Agakhanov, A.A.; Pautov, L.A.; Kasatkin, A.V.; Karpenko, V.Y.; Sokolova, E.; Day, M.C.; Hawthorne, H.C.; Muftakhov, V.A.; Pekov, I.V.; Cámara, F.; et al. Fluorapophyllite-(Cs), $CsCa_4Si_8O_{20}F{\cdot}8H_2O$, a new apophyllite-group mineral from the Darai-Pioz massif, Tien-Shan, northern Tajikistan. *Can. Mineral.* **2019**, *57*, 965–971. [CrossRef]
3. Števko, M.; Sejkora, J.; Plášil, J.; Dolníček, Z.; Škoda, R. Fluorapophyllite-(NH_4), $NH_4Ca_4Si_8O_{20}F{\cdot}8H_2O$, a new member of apophyllite group from Vechec quarry, eastern Slovakia. *Min. Mag.* **2020**, *84*, 533–539. [CrossRef]
4. Yang, H.; Gu, X.; Scott, M.M. Hydroxymcglassonite-(K), $KSr_4Si_8O_{20}(OH){\cdot}8H_2O$, the first Sr-bearing member of the apophyllite group, from the Wessels mine, Kalahari Manganese Field, South Africa. *Am. Mineral.* **2020**, *107*, 1818–1822. [CrossRef]
5. Matsueda, H.; Miura, Y.; Rucklidge, J. Natroapophyllite, a new orthorhombic sodium analog of apophyllite. I. Description, occurrence and nomenclature. *Am. Mineral.* **1981**, *66*, 410–4153.

6. Miura, Y.; Kato, T.; Rucklidge, J.; Matsueda, H. Natroapophyllite, a new orthorhombic sodium analog of apophyllite. II. Crystal structure. *Am. Mineral.* **1981**, *66*, 416–423.
7. Deer, W.A.; Howie, R.A.; Zussman, J. *Rock-Forming Minerals. Vol. 3. Sheet Silicates*; Longmans: London, UK, 1962; pp. 1–270.
8. Borisenko, Y.A. Occurrence and characteristics of apophyllite. *Min. Zh.* **1982**, *4*, 53–60. (In Russian)
9. Birch, W.D. Babingtonite, fluorapophyllite and sphene from Harcourt, Victoria, Australia. *Min. Mag.* **1983**, *47*, 377–380. [CrossRef]
10. Marincea, Ş. Mineralogical data concerning the magnesian hornfels in the Pietroasa area (Bihor Mountains). *Rom. J. Mineral.* **1993**, *76*, 29–41.
11. Włodika, R.; Wrzalik, R. Apophyllite from the Międzyrzecze sill near Bielsko-Biała, the type of area of the teschenite-picrite association. *Mineral. Polonica* **2004**, *35*, 19–32.
12. Suzuki, K.; Dunkley, D.J.; Kajizuka, I. Melanite from the endoskarn of a spessartite dyke intruding into the Kinshozan limestone in Ogaki City, Gifu Prefecture. *J. Earth Planet. Sci. Nagoya Univ.* **2011**, *58*, 1–29.
13. Cepedal, A.; Fuertes-Fuente, M.; Martin-Izard, A. Occurrence of silesiaite, a new calcium–iron–tin sorosilicate in the calcic skarn of El Valle-Boinás, Asturias, Spain. *Eur. J. Mineral.* **2021**, *33*, 165–174. [CrossRef]
14. Cioflica, G.; Vlad, Ş. The correlation of the Laramian metallogenetic events belonging to the Carpatho-Balkan area. *Rev. Roum. Géol. Géophys. Géogr. Sér. Géol.* **1973**, *17*, 217–224.
15. Săndulescu, M.; Kräutner, H.; Borcoş, M.; Năstăseanu, S.; Patrulius, D.; Ştefănescu, M.; Ghenea, C.; Lupu, M.; Savu, H.; Bercia, I.; et al. *Geological Map of Romania, Scale 1:1,000,000*; Institute of Geology and Geophysics: Bucharest, Romania, 1978.
16. Bleahu, M.; Soroiu, M.; Catilina, R. On the Cretaceous tectonic–magmatic evolution of the Apuseni Mountains as revealed by K–Ar dating. *Rev. Roum. Phys.* **1984**, *29*, 123–130.
17. Marincea, Ş. A contribution to the study of kotoite: Data on three Romanian occurrences. *N. Jb. Miner. Mh.* **2004**, *6*, 253–274. [CrossRef]
18. Marincea, Ş. Suanite in two boron-bearing magnesian skarns from Romania: Data on a longtime ignored mineral species. *N. Jb. Miner. Abh.* **2006**, *182/2*, 183–192. [CrossRef]
19. Marincea, Ş.; Dumitraş, D.-G. Contrasting types of boron-bearing deposits in magnesian skarns from Romania. *Ore Geol. Rev.* **2019**, *112*, 1–20. [CrossRef]
20. Berza, T.; Constantinescu, E.; Vlad, Ş.N. Upper Cretaceous magmatic series and associated mineralization in the Carpatho-Balkan Orogen. *Resour. Geol.* **1998**, *48*, 291–306. [CrossRef]
21. Ciobanu, C.L.; Cook, N.J.; Stein, H. Regional setting and geochronology of the Late Cretaceous Banatitic Magmatic and Metallogenetic Belt. *Miner. Depos.* **2002**, *37*, 541–567. [CrossRef]
22. Ilinca, G. Upper cretaceous contact metamorphism and related mineralizations in Romania. *Acta Min.-Petr. Abstr. Ser.* **2012**, *7*, 59–64.
23. Ştefan, A.; Roşu, E.; Andăr, A.; Robu, L.; Robu, N.; Bratosin, I.; Grabari, E.; Stoian, M.; Vîjdea, E. Petrological and geochemical features of Banatitic magmatites in Northern Apuseni Mountains. *Rom. J. Petrol.* **1992**, *75*, 97–115.
24. Ionescu, C.; Har, N. Geochemical considerations upon the banatites from Budureasa-Pietroasa area (Apuseni Mountains, Romania). *Stud. Univ. Babeş-Bolyai Geol.* **2001**, *46*, 59–80. [CrossRef]
25. Whitney, D.L.; Evans, B.W. Abbreviations for names of rock-forming minerals. *Am. Mineral.* **2010**, *95*, 185–187. [CrossRef]
26. Armstrong, J.T. Quantitative analysis of silicates and oxide minerals: Comparison of Monte Carlo, ZAF and Phi-Rho-Z procedures. In *Microbeam Analysis*; Newbury, D.E., Ed.; San Francisco Press: San Francisco, CA, USA, 1988; pp. 239–246.
27. Maxwell, J.A. Rock and Mineral Analysis. In *Chemical Analysis. A Series of Monographs on Analytical Chemistry and Its Applications*; Elving, P.J., Kolthoff, I.M., Eds.; Interscience Publishers: London, UK, 1968; Volume 27, pp. 1–584.
28. Appleman, D.E.; Evans, H.T., Jr. Indexing and least-squares refinement of powder diffraction data. *US Geol. Surv. Comput. Contrib.* **1973**, *20*, 60, (NTIS Doc. PB-216).
29. Benoit, P.H. Adaptation to microcomputer of the Appleman-Evans program for indexing and least-squares refinement of powder-diffraction data for unit-cell dimensions. *Am. Mineral.* **1987**, *72*, 1018–1019.
30. Agilent Technologies. *Xcalibur CCD System, CrysAlis Software System*; Agilent Technologies: Oxfordshire, UK, 2012.
31. Palatinus, L.; Chapuis, G. Superflip—A computer program for the solution of crystal structures by charge flipping in arbitrary dimensions. *J. Appl. Crystallogr.* **2007**, *40*, 786–790. [CrossRef]
32. Petříček, V.; Dušek, M.; Palatinus, L. Crystallographic computing system Jana2006: General features. *Z. Kristallogr.* **2014**, *229*, 345–352. [CrossRef]
33. Săbău, G.; Negulescu, E. Fluids strike back—Alkaline autometasomatism and peralkaline melt generation at the contact of the Măgureaua Vaţei pluton, South Apuseni Mountains. In *Geosciences in the 21st Century*; Segedi, A., Ilinca, G., Mocanu, V., Eds.; Geoecomar: Bucharest, Romania, 2019; pp. 189–191.
34. Pande, D.R.; Vadrabade, S.R. Etch pits on basal cleavage faces of apophyllite crystals. *Mineral. Mag.* **1990**, *54*, 559–565. [CrossRef]
35. Kostov, I. Apophyllite morphology as an example of habit modification of planar crystals. *N. Jb. Miner. Abh.* **1975**, *123*, 128–137.
36. Aldushin, K. Apophyllite Alteration in Aqueous Solutions. A Nano-Scale Study of Phyllosilicate Reactions. Unpublished Ph.D. Thesis, Ruhr-Universität Bochum, Bochum, Germany, 2004; pp. 1–95.
37. Dunn, P.J.; Rouse, R.C.; Norberg, J.A. Hydroxyapophyllite, a new mineral, and a redefinition of the apophyllite group. I. Description, occurrences and nomenclature. *Am. Mineral.* **1978**, *63*, 196–199.

38. Larsen, A.O. Hydroxyapophyllite from the Mofjellet mine, Mo i Rana, northern Norway. Contributions to the mineralogy of Norway, No. 66. *Norsk Geologisk Tidsskrift* **1981**, *61*, 297–300.
39. Belsare, M.R. A chemical study of apophyllite from Poona. *Min. Mag.* **1969**, *37*, 288–289. [CrossRef]
40. Colville, A.A.; Anderson, C.P. Refinement of the crystal structure of apophyllite. I. X-ray diffraction and physical structure. *Am. Mineral.* **1971**, *56*, 1222–1233.
41. Abidoğlu, E. Mineralogy and chemistry of zeolites and associated minerals in Tertiary alkaline volcanics from the Eastern Pontides, NE Turkey. *N. Jb. Miner. Abh.* **2011**, *188/1*, 35–47.
42. Taylor, W.H.; Naray-Szabo, S. The structure of apophyllite. *Z. Kristallogr.* **1931**, *77*, 146–158. [CrossRef]
43. Chao, G.Y. Refinement of the crystal structure of apophyllite. II. Determination of the hydrogen positions by X-ray diffraction. *Am. Mineral.* **1971**, *56*, 1234–1242.
44. Prince, E. Refinement of the crystal structure of apophyllite III. Determination of the hydrogen positions by neutron diffraction. *Am. Mineral.* **1971**, *56*, 1243–1251.
45. Bartl, H.; Pfeifer, G. Neutronenbeigungs-analyse des Apophyllite $KCa_4(Si_4O_{10})_2(F/OH)\cdot 8H_2O$. *N. Jb. Miner. Mh.* **1976**, *2*, 58–65.
46. Pechar, F. An X-ray diffraction refinement of the crystal structure of natural apophyllite. *Cryst. Res. Technol.* **1987**, *22*, 1041–1046. [CrossRef]
47. Ståhl, K.; Kvick, Å.; Ghose, S. A neutron diffraction and thermogravimetric study of the hydrogen bonding and dehydration behaviour in fluorapophyllite, $KCa_4(Si_8O_{20})F\cdot 8H_2O$, and its partially dehydrated form. *Acta Crystallogr.* **1987**, *B43*, 517–523. [CrossRef]
48. Ståhl, K. A neutron powder diffraction study of partially dehydrated fluorapophyllite, $KCa_4Si_8O_{20}F\cdot 6.9H_2O$. *Eur. J. Mineral.* **1993**, *5*, 845–849. [CrossRef]
49. Rouse, R.C.; Peacor, D.R.; Dunn, P.J. Hydroxyapophyllite, a new mineral, and a redefinition of the apophyllite group. II. Crystal structure. *Am. Mineral.* **1978**, *63*, 199–202.
50. Brănoiu, G.; Cursaru, D.; Mihai, S.; Ramadan, I. Rietveld structure refinement of the apophyllite crystals from Deccan Basalt Plateau using X-ray powder diffraction data. *Rev. Chim.* **2019**, *70*, 4248–4254. [CrossRef]
51. Brown, I.D.; Altermatt, D. Bond-valence parameters obtained from a systematic analysis of the Inorganic Crystal Structure Database. *Acta Crystallogr.* **1985**, *B41*, 244–247. [CrossRef]
52. Gagné, O.C.; Hawthorne, F.C. Comprehensive derivation of bond-valence parameters for ion pairs involving oxygen. *Acta Crystallogr.* **2015**, *B71*, 562–578. [CrossRef]
53. Mittra, D.; Ali, S.Z. Crystal data for apophyllite. *J. Appl. Crystallogr.* **1976**, *9*, 54–56. [CrossRef]
54. Marriner, G.F.; Tarney, J.; Langford, J.I. Apophyllite group: Effects of chemical substitutions on dehydration behaviour, recrystallization products, and cell parameters. *Min. Mag.* **1990**, *55*, 567–578. [CrossRef]
55. Fan, D.-W.; Wei, S.-Y.; Xie, H.-S. An in situ high-pressure X-ray diffraction experiment on hydroxyapophyllite. *Chin. Phys. B* **2013**, *22/1*, 010702. [CrossRef]
56. Kim, Y.-H.; Choi, J.; Heo, S.; Jeong, N.; Hwang, G.C. High pressure behavior study of the apophyllite (KF). *J. Mineral. Soc. Korea* **2015**, *28*, 325–332. [CrossRef]
57. Sidey, V. On the effective ionic radii for ammonium. *Acta Crystallogr. B Struct. Sci. Cryst. Eng. Mater.* **2016**, *72*, 626–633. [CrossRef]
58. Shannon, R.D. Revised effective ionic radii and systematic studies on interatomic distances in halides and chalcogenides. *Acta Crystallogr.* **1976**, *A32*, 751–767. [CrossRef]
59. Mandarino, J.A. The Gladstone-Dale relationship—Part I: Derivation of new constants. *Can. Mineral.* **1976**, *14*, 498–502.
60. Mandarino, J.A. The Gladstone-Dale relationship. IV. The compatibility concept and its application. *Can. Mineral.* **1981**, *19*, 441–450.
61. Koizumi, M. The differential thermal analysis curves and hydration curves of zeolites. *Mineral. J. Jap.* **1953**, *1*, 36–47. [CrossRef]
62. Young, B.; Dyer, A.; Hubbard, N.; Starkey, R.E. Apophyllite and other zeolites-type minerals from the Whin Sill of the northern Pennines. *Min. Mag.* **1991**, *55*, 203–207. [CrossRef]
63. Frost, R.L.; Xi, Y. Thermoanalytical study of the minerals apophyllite-(KF) $KCa_4Si_8O_{20}F\cdot 8H_2O$ and apophyllite-(KOH) $KCa_4Si_8O_{20}(F,OH)\cdot 8H_2O$. *J. Therm. Anal. Calorim.* **2013**, *112*, 607–614. [CrossRef]
64. Ryskin, Y.I.; Stavitskaya, G.P. Asymmetry of the water molecule in crystal hydrates: IR spectra of dioptase and apophyllite. *Izv. Akad. Nauk SSSR Ser. Khim.* **1990**, *8*, 1778–1782. [CrossRef]
65. Sidorov, T.A. The molecular structure and vibrational spectrum of apophyllite $KCa_4(Si_8O_{20})(F,OH)\cdot 8H_2O$. *Russ. J. Phys. Chem.* **2000**, *74*, 449–453.
66. Frost, R.L.; Xi, Y. Raman spectroscopic study of the minerals apophyllite-(KF) $KCa_4Si_8O_{20}F\cdot 8H_2O$ and apophyllite-(KOH) $KCa_4Si_8O_{20}(F,OH)\cdot 8H_2O$. *J. Mol. Struct.* **2012**, *1028*, 200–207. [CrossRef]
67. Seryotkin, Y.V.; Kupriyanov, I.N.; Ignatov, M.A. Single-crystal X-ray diffraction and IR-spectroscopy studies of potassium-deficient fluorapophyllite-(K). *Phys. Chem. Miner.* **2023**, *50*, 6. [CrossRef]
68. Adams, D.M.; Armstrong, R.S.; Best, S.P. Single-crystal Raman spectroscopic study of apophyllite, a layer silicate. *Inorg. Chem.* **1981**, *20*, 1771–1776. [CrossRef]
69. Goryainov, S.V.; Krylov, A.S.; Pan, Y.; Madyukov, Y.A.; Smirnov, M.B.; Vtyurin, A.N. Raman investigation of hydrostatic and nonhydrostatic compressions of OH- and F-apophyllites up to 8 GPa. *J. Raman. Spectrosc.* **2012**, *43*, 439–447. [CrossRef]

70. Ogorodova, L.P.; Melchakova, L.V.; Vigasina, M.F.; Grytsenko, Y.D.; Ksenofontov, D.A.; Bryzgalov, I.A. Thermodynamic properties of fluorapophyllite-(K) and hydroxyapophyllite-(K). *Geochem. Internat.* **2019**, *57*, 805–811. [CrossRef]
71. Libowitzky, E. Correlation of O-H stretching frequencies and O-H...O hydrogen bond lengths in minerals. *Monatsh. Chem.* **1999**, *130*, 1047–1059. [CrossRef]
72. Ryskin, Y.I. The vibration of protons in minerals: Hydroxyl, water and ammonium. In *The Infrared Spectra of Minerals*; Farmer, V.C., Ed.; Mineralogical Society Monograph 4: London, UK, 1974; pp. 137–182.
73. Coates, J. Interpretation of Infrared Spectra, a Practical Approach. In *Encyclopedia of Analytical Chemistry*; Meyers, R.A., Ed.; John Wiley & Sons Ltd.: Chichester, UK, 2000; pp. 10815–10837.
74. Jon, H.; Lu, B.; Oumi, Y.; Itabashi, K.; Sano, T. Synthesis and thermal stability of beta zeolite using ammonium fluoride. *Microporous Mesoporous Mat.* **2006**, *89*, 88–95. [CrossRef]